Multiorder rotating grating interferometer

John Howard

A multichannel interferometer that uses a rotating grating to both disperse and Doppler shift an incident far-infrared laser beam is described. The laser beam is diffracted into a fan array of many (~ 10) beams that can be directed to probe the plasma along distinct chords. The phase-shift information is multiplexed in the frequency domain so that a single detector suffices to sense the recombined probing beams.

Key words: Interferometry, diffraction gratings.

I. Introduction

Infrared and far-infrared radiation beams are routinely employed to sense the density of electrons in magnetically confined plasmas.[1–3] The phase of the probing beam ϕ is shifted in proportion to the integral of the electron density n_e along the laser-beam line of sight.[4] Interferometric measurements of the phase shift for beams at a number of viewing angles and impact parameters allow, in principle, the density profile to be recovered approximately by using tomographic techniques.[5]

A multichannel far-infrared scanning interferometer for two-dimensional plasma density measurements was described recently.[6] The instrument makes use of a multisectored blazed disk grating. When the wheel is rotated, the beam that is incident on the wheel edge is diffracted sequentially through a range of discrete angles to probe the plasma at a set of fixed impact parameters, the diffracted beam angle being determined by the grating constant of the illuminated sector. Because of this multiplexing in time, many spatial channels can be obtained by using a single laser beam and detector. However, time resolution is necessarily compromised for the spatial scanning capability.

In this paper we report the successful construction and operation of a multiorder grating interferometer. The beam that is incident on the grating wheel circumference in this case is diffracted simultaneously into many fixed orders, at angles that are determined by the grating equation. When the wheel is rotated the diffracted beams are Doppler shifted in proportion to their order number so that the spatial information that is encoded by each probe beam is multiplexed in the frequency domain (rather than in time). This restores the continuous time resolution while still allowing simultaneous multichannel phase-shift information to be obtained by using only a single laser beam and probe beam detector.

In Section II we outline the principle of the device and discuss some of the more important design issues. A mode-matching method[7,8] is used to calculate the grating performance in Section III, and the experimental results, which are in excellent agreement with theory, are presented in Section IV. Finally in Section V we discuss possible interferometric applications of the device, and results that were obtained by using a prototype interferometer are described.

II. Principle

A. Background

The mth-order angle of diffraction θ_m for a plane electromagnetic wave ($\lambda_0 = 2\pi/k_0$, $\omega_0 = ck_0$) incident at angle θ_i on an infinite plane grating with groove spacing $d = 2\pi/K$ is given by

$$\sin \theta_m = \sin \theta_i + mK/k_0. \tag{2.1}$$

This grating equation, together with a simple ray optics analysis, has been used to account successfully for the reflection behavior of a Gaussian beam that is incident on the edge, and in a plane normal to the axis, of the circular scanning grating wheel[6] (see Fig. 1 for the geometry). When the wheel is rotated, the radiation is Doppler shifted in angular frequency by

$$\Omega_m = mKR\omega \cos \gamma, \tag{2.2}$$

where R is the wheel radius, ω is the wheel angular

The author is with the Plasma Research Laboratory, Research School of Physical Sciences, The Australian National University, Canberra, ACT 2601, Australia.

Received 3 December 1990.
0003-6935/92/101419-07$05.00/0.

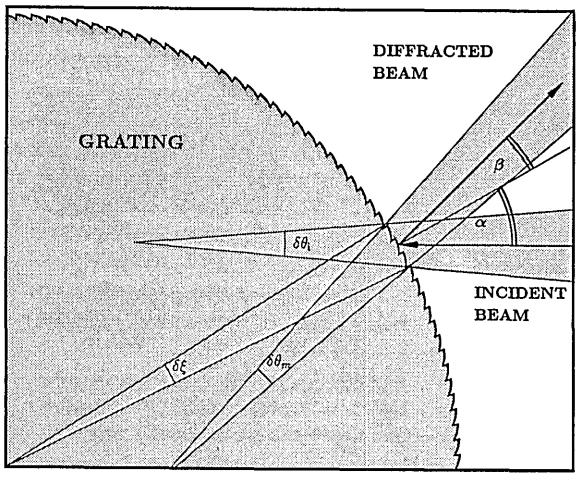

Fig. 1. Diffraction geometry showing relationship between incident and reflected rays.

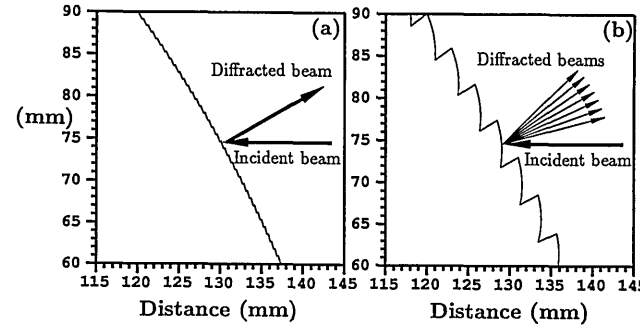

Fig. 2. Groove profiles for (a) scanning and (b) multiorder (#3) gratings.

rotation frequency, and γ is the angle between the incident beam and the plane containing the grating wheel (from now on we take $\gamma = 0$). When the diffracted beam is mixed with some of the unshifted radiation in a nonlinear detector a signal at the intermediate frequency (IF) Ω_m results. This IF carrier can be demodulated to recover the phase shift that is suffered by the probe beam after passage through the plasma. For this reason rotating grating wheels were previously used exclusively as Doppler shifting elements for heterodyne detection in far-infrared plasma scattering and interferometry experiments.[1] Notice, however, that both Ω_m and θ_m depend on the diffraction order m. If the grating groove profile can be tailored to generate a fan array of N sufficiently closely spaced probe beams (θ_m; $m = m_1, m_2, \ldots, m_N$), each of the resulting distinct plasma spatial channels will be tagged by Ω_m. Under the conditions specified in Section IV, all the probe beams can be mixed in a single detector and the phase information $\phi_m(t)$ that is carried by the mth-order beam can be retrieved unambiguously.

B. Design considerations

The scanning grating wheel (which is described in Ref. 6) uses triangular groove profiles that are blazed to reflect specularly into first order with a measured efficiency of $\sim 90\%$. In a natural extrapolation, the groove profile for the multiorder grating is constructed of N smaller, flat subfacets, with adjacent subfacets incrementally inclined to reflect specularly into the next highest order. The width of the subfacets is fixed so that each presents the same surface area to the incident beam. In this way, none of the required diffracted orders should be preferred to any other. Typical groove profiles for both scanning and multiorder wheels are shown in Fig. 2.

To probe the plasma, the N-diffracted beams should be clustered within a narrow range of angles (say $\lesssim 30°$). This requires that the groove spacing d be substantially greater than λ_0. However a sufficient number of grooves G must be illuminated (which requires small d) to ensure that the grating reflectivity is not modulated at the groove frequency; such modulation of the IF signal would introduce destructive sidebands at the difference frequency Ω_1 between adjacent carriers Ω_m. This is a potential difficulty for an interferometer that is based on this type of grating.

For a laser beam of spot diameter W at the grating surface, the number of illuminated grooves is $G \sim a/d$ where $a = W/\cos\theta_i$ is the major diameter of the elliptical illuminated region. [We take $W = 2w$, where w is the radius at which the intensity has fallen to exp (-1) of its peak value.] Although G increases for larger incidence angles, departure from collimation of the diffracted beams can be a problem if θ_i becomes too great. To ensure good collimation of the reflected beams ($\delta\theta_m = 0$; see Fig. 1), the beam that is incident on the wheel must be sufficiently tightly focused to compensate for the wheel curvature. Some geometry shows that this requires that the ratio of the incident convergence angle $\delta\theta_i$ to the angle $\delta\xi$ that is subtended by a at the wheel center be equal to the quantity μ_m, where $\mu_m = \cos\theta_m/\cos\theta_i$ is fixed by the reflection geometry. If the collimation condition is satisfied for the central beam in the fan array ($\theta_m = \theta_c$), the divergence angle for beams at other angles is

$$\delta\theta_m = \delta\xi\left(1 - \frac{\cos\theta_c}{\cos\theta_m}\right) \tag{2.3}$$

and is most significant when the incidence angle is large [$\delta\xi = W/(R\cos\theta_i)$]. Therefore a larger number G of illuminated grooves (and hence a) is most satisfactorily obtained either by using a low f-number coupling onto the wheel surface (i.e., large $\delta\theta_i$) or by increasing the radius of the wheel.

III. Theoretical Description

To calculate the power distribution among the propagating orders, we consider the idealized problem of plane-wave diffraction from a perfectly conducting plane grating. This ignores the Gaussian nature of the beam and the curvature of the grating surface. The grating, which is taken to occupy the space $y < 0$, is uniform in the z direction (parallel to the wheel axis) and has a profile $y = \eta(x)$ that is periodic in the x direction with period d. The cross section of the

groove surface is shown in Fig. 2 (see also Fig. 5 below). Being composed of piecewise linear segments (or subfacets), a point $s = (x, y)$ on the groove surface L is defined by

$$y = \eta(x) = \sum_{q=1}^{Q} F_q(\alpha_q x + \beta_q), \tag{3.1}$$

where F_q is unity in the region of the qth subfacet and zero elsewhere.

For an incident unit-amplitude plane wave with a wave vector in the x–y plane, it is sufficient to consider the P and S polarizations for the electric field vector $\mathbf{E}$. In the latter case, the magnetic intensity $\mathbf{H}$ is parallel to the grooves and we can write

$$\mathbf{H}_i = \hat{k}\,\Psi_i(x, y), \tag{3.2}$$

where $\hat{k}$ is the unit vector in the z direction and the time dependence $\exp(-j\omega_0 t)$ is assumed. For an incident plane wave, we have

$$\Psi_i(x, y) = \exp(jk_{ix}x + jk_{iy}y), \tag{3.3}$$

$$(k_{ix}, k_{iy}) = k_0(\sin\theta_i, -\cos\theta_i). \tag{3.4}$$

The same form Ψ_i describes the variation of the z component of the $\mathbf{E}$ field in the P-polarization case.

In the free-space region $y > 0$, the z component of the reflected field Ψ_r can be expanded by using an infinite series of plane-wave modal functions.[7,8] We denote the complex field amplitudes by H_m, and we have for the S polarization

$$\Psi_r = \sum_{m=-\infty}^{\infty} H_m \psi_m(x, y), \tag{3.5}$$

where

$$\psi_m(x, y) = \exp(jk_{mx}x + jk_{my}y), \tag{3.6}$$

$$k_{mx} = k_{ix} + mK,$$
$$k_{my} = (k_0^2 - k_{mx}^2)^{1/2}, \tag{3.7}$$

with $\mathrm{Im}(k_{my})$ and $\mathrm{Re}(k_{my}) \geq 0$. In the P polarization the complex amplitudes are denoted by E_m. When k_{my} is real (propagating waves), the plane wave ψ_m represents the mth spectral order that is propagating at angle θ_m to the y axis with fractional energy $\epsilon_m = (k_{my}/k_{0y})|H_m|^2$.

At the grating surface the boundary conditions

$$\Psi_r(s) = -\Psi_i(s), \tag{3.8}$$

$$\frac{\partial\Psi_r(s)}{\partial\nu} = -\frac{\partial\Psi_i(s)}{\partial\nu} \tag{3.9}$$

apply, respectively, for the P- and S-polarized waves, where $\partial/\partial\nu$ denotes the normal derivative on the groove surface L. In general, however, the expansion equation (3.5) for Ψ_r is not valid in the valley of the groove between the x axis and the grating surface, so matching Eqs. (3.3) and (3.5) through the boundary conditions Eqs. (3.8) and (3.9) does not guarantee an accurate solution.[9] It is, however, possible to approximate the diffracted field in the region $y > \eta(x)$ by a finite series of the form

$$\Psi_r^{(M)} = \sum_{m=-M}^{m=M} H_m^{(M)} \psi_m(x, y) \tag{3.10}$$

and to obtain the amplitudes $H_m^{(M)}$ by matching the boundary condition [Eq. (3.9)] in the least-squares sense (the so-called mode-matching or Yasuura method).[7,8] Although the coefficients $H_m^{(M)}$ are dependent on the number of terms $2M + 1$ in the series approximation, they approach the true coefficients as M becomes large. A necessary (but not sufficient[10]) measure of this convergence is a departure from the energy conservation $1 - \Sigma_m' \epsilon_m^{(M)}$, where the prime indicates that the sum is over the propagating components only. For the calculations that are presented below, the number of expansion terms $2M + 1 \leq 60$ is sufficient to ensure energy conservation to at least 3%, and usually to better than 1%. As a further check on the convergence, we calculate the quantity

$$\delta^{(M)} = \frac{1}{M_p} \sum_{m=-M}^{m=M}{}' \frac{|H_m^{(M)} - H_m^{(M-1)}|^2}{|H_m^{(M)}|^2}, \tag{3.11}$$

where M_p is the number of propagating orders. This is a measure of the variation with M of the average change in the energy that is diffracted into the propagating orders. Typically it is found that $\delta^{(M)}$ decreases monotonically to $\sim 10^{-3}$ for M up to $M \sim 30$, and saturates at a minimum value of $\sim 10^{-4}$ for $M \gtrsim 40$.

IV. Performance

Three test grating sections of 30-mm lengths were cut by using a numerically controlled wire-discharge machine on the edge of an aluminum disk of modest radius $R = 150$ mm and 20-mm thickness. The groove profiles were designed for a 50-mW hydrogen cyanide (HCN) laser source[11] ($\lambda_0 = 337$ μm) that was focused onto the wheel at an incidence angle $\theta_i = 45°$. Taking $\theta_c \approx 0$ allows adequate separation of the incident and reflected beams, while modest fan angles are chosen to minimize the spread in diffracted beam divergence. Within these general constraints, grooves with the following specifications were cut and their reflection properties measured:

Pattern #1:	$d = 4$ mm,	$(m_1, m_N) = (4, 15)$;
Pattern #2:	$d = 4$ mm,	$(m_1, m_N) = (6, 14)$;
Pattern #3:	$d = 5$ mm,	$(m_1, m_N) = (6, 18)$.

The typical profile shape is illustrated in Fig. 2.

The diffracted beam profiles were measured by translating a pyroelectric detector across the diffracted radiation at a fixed distance z from the grating and using synchronous detection techniques. The incident radiation was polarized at 90° to the grooves (S polarization). The measured convergence angle onto the grating was $\delta\theta_i = 15 \pm 1°$. The best reflected

beam collimation was achieved with a spot size $W = 9.0 \pm 0.5$ mm. The spot diameter that is required for collimation according to the simple-minded theory of Subsection II.B is $W = 11 \pm 1$ mm.

The reflected power distribution at $z = 0.3$ m for groove profiles #1–#3 are presented in Fig. 3. The curves have been normalized so that the sum of the energies in the measured orders is unity. The measured spread in reflection efficiencies between the patterns is less than 5%. The reflected beams appear to emanate from a spot on the wheel of a diameter $W_m = \mu_m W$. Beyond the Rayleigh range $z_R = k_0 W_m^2/4$, the diffracted beam has constant divergence $\delta\theta_m = k_0 W_m/2$. For the central beam, $z_R \sim 0.4$ m and $\delta\theta_c \sim 0.7°$ are less than the angular separation between beams ($\sim 4°$). A larger diameter wheel would allow larger spot diameters with a better reflected beam collimation, which is necessary for longer propagation paths.

The sets of vertical bars superimposed upon the measured profiles in Fig. 3 show the computed power distribution among the diffracted orders obtained by using the Yasuura method. The closest fit with experiment is obtained for an incidence angle $\theta_i = -47°$ (within the measurement uncertainty for the nominal experimental incidence angle $\theta_i = -45°$). The angular positions of the beams are consistent with the grating equation [Eq. (2.1)]. When comparing Figs. 3(b) and 3(c) we note that, as expected, the diffracted beams are clustered more closely for the $d = 5$-mm grating (#3).

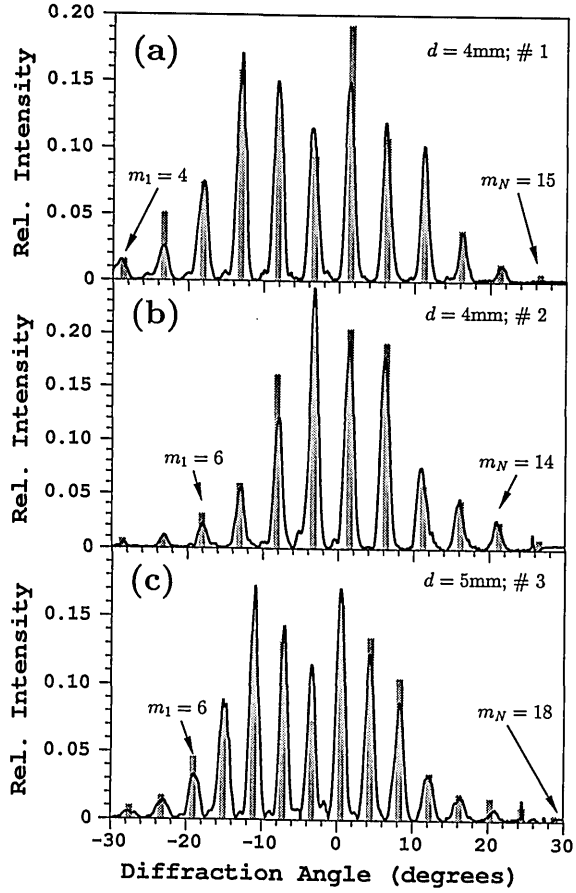

Fig. 3. Measured reflected beam profiles for groove patterns #1–#3 at a distance 0.3 m from the grating. The superimposed gray bars show the computed relative intensities, and the positions of the minimum and maximum design orders m_1 and m_N are indicated on the plot.

Because of the shadowing effect of the groove vertex, the higher-order beams in each case are extinguished for values of m less than the design cutoff m_N. Numerically this has been taken into account by projecting the vertex onto the adjacent groove surface in the direction of the incident wave (for example, compare Fig. 2 with Fig. 5 below). The power in the lower orders also diminishes dramatically as the design cutoff is approached. Note especially the marked contrast between the low-order reflectivity of profiles #1 ($m_1 = 4$) and #2 ($m_1 = 6$).

In general the features of the reflected distributions conform well with theory. The observed discrepancies may be attributable to several sources. First, the computed results should be compared strictly with the integrated power in each diffracted order. This is a small correction that tends to increase the peak intensity of the beams at larger diffraction angles by $\leq 10\%$ [see Eq. (2.3)]. Given the nominal 5-μm machining accuracy of the groove profiles, computations suggest that random profile errors can only in small part account for the observed differences. On the other hand, it has been observed that the reflected intensity in a given order can vary by as much as $\sim 10\%$, depending on the position of the grooves relative to the incident beam. This is due to the small number of illuminated grooves—an effect not accommodated by the plane-wave mode-matching method. This problem is considered in relation to interferometry in Section V. Another possible source of error is that the simple expedient of projecting the vertex onto the adjacent groove (i.e., filling the region in the shadow of the groove vertex with a conductor) ignores possibly important diffraction effects in this region. More extensive calculations and measurements to resolve these issues are planned.

Figure 4 shows the computed reflectivities for a grating with design parameters as for pattern #1 above, but with the elimination of the shadow region. This modified pattern #1 is shown (for a design incidence angle $-45°$) in Fig. 5. The calculated P and S reflectivities (for $\theta_i = -45°$) are shown, respectively, in Figs. 4(a) and 4(b). Note that all the design orders from $m_1 = 4$ to $m_N = 15$ are now evident though the power distributions in the two polarizations are significantly different. Computations show that this type of grating can also be used for a wide range of incidence angles. For example, for $\theta_i = -55°$ and S polarization [Fig. 4(c)] the reflected beams are of comparable intensity, the cluster being shifted in accordance with the specular nature of the reflecting surface. To verify this behavior, we have measured the reflected power distribution for pattern #1 in the case for which θ_i is increased by 2° to $\theta_i = -45°$. As illustrated in Fig. 6,

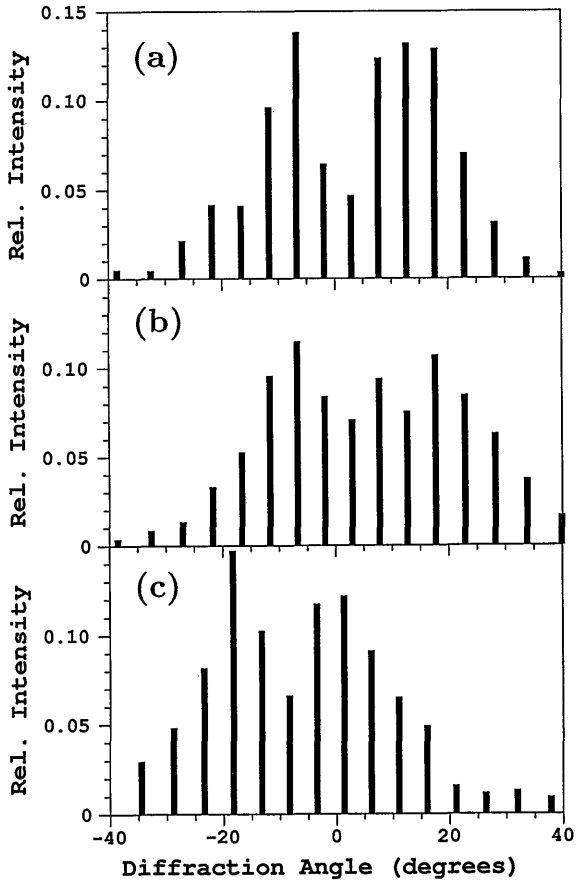

Fig. 4. Computed reflected beam intensities for modified groove pattern #1 for (a) $\theta_i = -45°$, P polarization; (b) $\theta_i = -45°$, S polarization; and (c) $\theta_i = -55°$, S polarization.

there is good agreement between the measured and computed power distributions.

The correspondence between observation and design lends some support to the blazed subfacets approach to groove profile design. Encouraged by the generally convincing agreement between the measurements and mode-matching computations, we are investigating the use of the theory for the design of an optimal element that reflects equal power into the design orders. This would be the reflection analog of the Dammann transmission grating.[12]

V. Interferometry

As noted above, it is an advantage to combine all the probe beams on a single detector. At the detector we write for the local oscillator (LO) field

$$u_{LO} = a_{LO} \exp(j\omega_{LO}t), \tag{5.15}$$

where $\omega_{LO} = \omega_0 + \Omega_{LO}$, and a_{LO} is the field amplitude. For our purposes, it suffices to consider two constant amplitude probe beams:

$$u_1 = a_1 \exp[j\omega_1 t + j\phi_1(t)],$$
$$u_2 = a_2 \exp[j\omega_2 t + j\phi_2(t)], \tag{5.1}$$

where $\omega_n = \omega_0 + n\Omega_1$, and $\Omega_1/(2\pi)$ is the difference

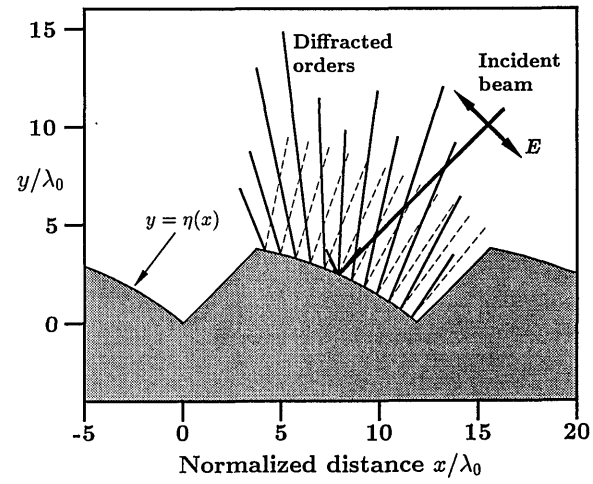

Fig. 5. Diagram showing reflection of diffracted orders from the successively inclined subfacets that constitute the modified piecewise linear grating profile #1. The nonreflecting surface is parallel to the incident wave vector (heavy line). The lengths of the solid lines emanating from the center of each subfacet represent the relative reflected beam intensities (S polarization), while the dashed lines are the subfacet normals. Radiation in orders not corresponding to one of the subfacets is shown as emanating from the groove center.

frequency between adjacent orders. For simplicity, we ignore nonplasma-related phase shifts. The detector signal is proportional to

$$i(t) = |u_1(t) + u_2(t) + u_{LO}(t)|^2, \tag{5.2}$$

the time-varying part of which is given by

$$\tilde{i}(t) = a_{LO}a_1 \cos[(\Omega_{LO} - \Omega_1)t - \phi_1(t)] + a_{LO}a_2 \cos[(\Omega_{LO} - 2\Omega_1)t - \phi_2(t)] + a_1a_2 \cos[\Omega_1 t + \phi_1(t) - \phi_2(t)]. \tag{5.3}$$

When the local oscillator is unshifted ($\Omega_{LO} = 0$), then unless $a_{LO} \gg a_1$, interference will occur between the carrier component $a_{LO}a_1$ and the intermodulation term a_1a_2. There are a number of solutions to this

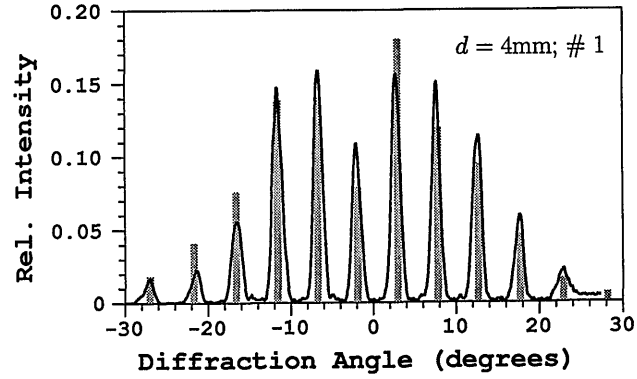

Fig. 6. Measured reflected beam profile for groove pattern #1 at a distance 0.3 m from the grating and incidence angle −45°. The superimposed gray bars show the corresponding computed relative intensities.

problem. The most satisfactory solution is to avoid the possibility of interference by choosing the minimum and maximum orders so that $m_1 > (m_N - m_1)$. If this is impractical, another possibility is to mix ω_0 only with odd-order beams and to select one of the odd-order beams as local oscillator for the even-order beams. This, however, necessitates physical separation of the beams. A more satisfactory approach is to provide a local oscillator that is offset from ω_0 by an account Ω_{LO} that is not equal to a multiple of the difference frequency Ω_1. This could be obtained by illuminating the grating at some angle γ to the plane of the wheel. Alternatively the local oscillator could be derived from another grating wheel coaxial with the primary wheel.

The plasma phase can be unambiguously recovered, provided $\Omega_p < |(\Omega_{LO} - n\Omega_1)|$, where Ω_p represents the effective bandwidth of the plasma phase $\phi(t)$. To avoid channel cross talk, we further require that $\Omega_p < \Omega_1/2$. For test grating #1 and wheel rotation at 6000 rpm, phase variations to a bandwidth of ~12 kHz can be unambiguously recovered. In practice, this could be done by using bandpass filters and analog phase detectors or by appropriate digital signal processing techniques.[13] We remark that, for extraction of reliable plasma phase-shift information, it may be necessary (for example, when Ω_1 varies with time) to furnish a suitable phase base line. This could be derived from one of the outer diffracted beams or obtained directly by sampling the entire diffracted profile by using a beam splitter.

A test Mach–Zehnder interferometer (which is shown schematically in Fig. 7) has been constructed to test the wheel modulation performance. The ratio of local oscillator and probe beam powers can be optimized by varying the orientation of the first polarizing beam splitter. The polarization transforming reflectors[14] (PTR's) and the mixing polarizer are subsequently adjusted to maximize the pyroelectric detector signal. The asymmetric reflection properties of the wheel are compensated for by using appropriate cylindrical optics.

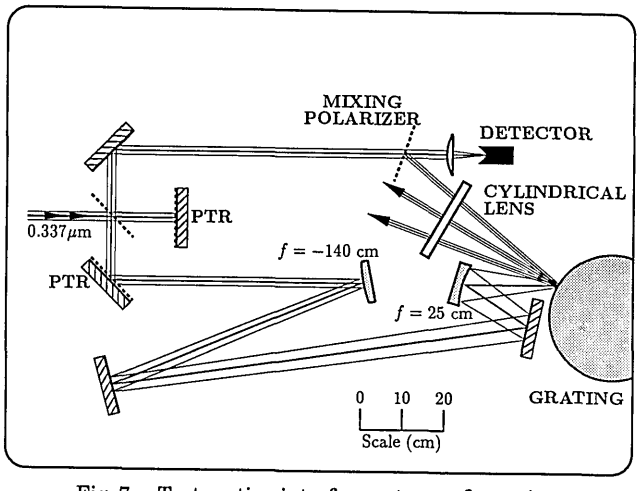

Fig. 7. Test grating interferometer configuration.

As commented earlier, of concern is possible amplitude modulation of the reflected probe beam. The introduced sidebands occur at frequencies that are shifted by $\pm\Omega_1$ from the carrier, regardless of the mixing process. Figure 8 shows the IF signal bursts that are obtained by mixing the ninth-order diffracted beams from ruled sectors #1 and #3 with part of the laser output. It is perhaps surprising, given that the spot at the grating surface illuminates only ~3 grooves, that the observed modulation is, if not insignificant, at least tolerably small (see Fig. 8). The situation would undoubtedly improve for larger spot diameters. As expected, the signal frequency is nine times the groove modulation frequency. It has been confirmed that the other diffracted components also obey Eq. (2.2).

The use of a Michelson configuration, where the diffracted beams execute a double pass of the grating surface, has not been explored. In passing, we note that a possible hybrid grating that incorporates both multiorder grooves and a spatial scanning capability, could in some circumstances represent a convenient compromise between dense spatial sampling and time resolution.

It is a pleasure to acknowledge the skills and generosity of P. Paculla, J. Crowhurst, B. Morales,

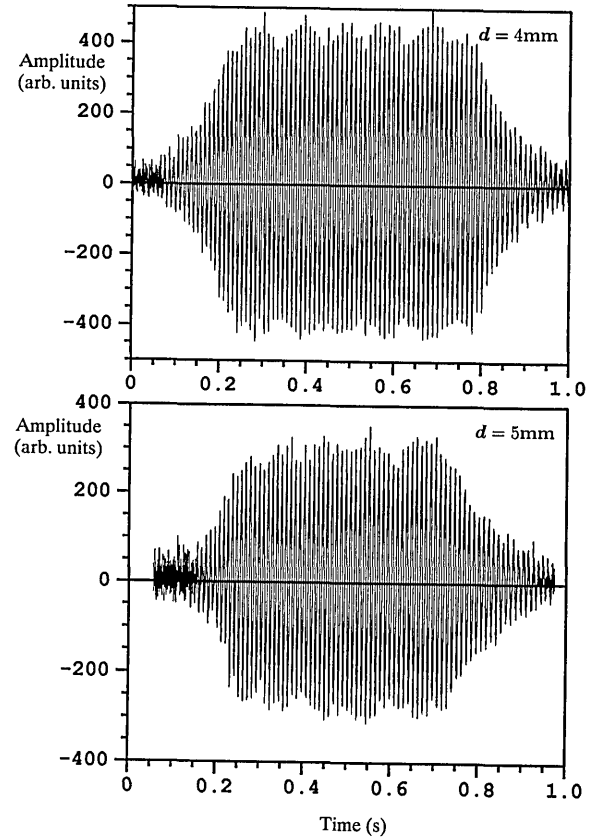

Fig. 8. Fringe bursts from the ninth-order diffracted beam for d = 4-mm (#1) and d = 5-mm (#3) grooves. In each case, the intermediate frequency is nine times greater than the small amplitude modulation at the groove frequency.

and P. Alexander of the Royal Australian Mint for their part in fabricating the reflection grating. Thanks are due to G. B. Warr, P. C. Hill, and R. C. McPhedran for useful discussions. Finally, the author thanks S. M. Hamberger for provision of the excellent facilities required to carry out this work.

References

1. D. Veron, 'High sensitivity HCN laser interferometer for plasma electron density measurements," Opt. Commun. **10,** 95–98 (1974).
2. P. E. Young, D. P. Neikirk, P. P. Tong, D. B. Rutledge, and N. C. Luhmann, Jr., "Multichannel far-infrared phase imaging for fusion plasmas," Rev. Sci. Instrum. **56,** 81–89 (1984).
3. W. A. Peebles, R. L. Savage, D. L. Brower, S. K. Kim, T. Lehecka, J. Howard, E. J. Doyle, and N. C. Luhmann Jr., "Plasma diagnostic applications on the TEXT Tokamak using a high-power twin-frequency optically pumped far-infrared laser," Int. J. Infrared Millimeter Waves **8,** 1355–1363 (1987).
4. D. Veron, "Submillimeter interferometry of high density plasmas," in *Infrared and Millimeter Waves,* K. J. Button, ed. (Academic, New York, 1979), Vol. 2, pp. 69–135.
5. J. Howard, E. J. Doyle, G. Reibeiz, R. L. Savage, W. A. Peebles, and N. C. Luhmann, Jr., "Density profile reconstructions from 2-D interferometric data on microtor using novel tomographic analysis techniques," Rev. Sci. Instrum. **59,** 2135–2138 (1988).
6. J. Howard, "Novel scanning interferometer for two-dimensional plasma density measurements," Rev. Sci. Instrum. **61,** 1086–1094 (1990).
7. H. Ikuno and K. Yasuura, "Improved point matching method with application to scattering from a periodic structure," IEEE Trans. Antennas Propagat. **AP-21,** 657–662 (1973).
8. T. Matsuda and Y. Okuno, "Computer-aided algorithm based on the Yasuura method for analysis of diffraction by a grating," J. Opt. Soc. Am. A **7,** 1693–1700 (1990).
9. J. P. Hugonin, R. Petit, and M. Cadilhac, "Plane wave expansions used to describe the field diffracted by a grating," J. Opt. Soc. Am. **71,** 593–598 (1981).
10. N. Amitay and V. Galindo, "On energy conservation and the method of moments in scattering problems," IEEE Trans. Antennas Propagat. **AP-17,** 747–751 (1969).
11. L. B. Whitbourn, "A 337 μm density interferometer for the LT4 Tokamak," Int. J. Infrared Millimeter Waves **5,** 625–635 (1984).
12. H. Dammann and K. Görtler "High-efficiency in-line multiple imaging by means of multiple phase holograms," Opt. Commun. **3,** 312–315 (1971).
13. D. W. Choi, E. J. Powers, R. D. Bengston, G. Joyce, D. L. Brower, N. C. Luhmann, Jr., and W. A. Peebles, "Digital complex demodulation applied to interferometry," Rev. Sci. Instrum. **57,** 1989–1991 (1986).
14. J. Howard, W. A. Peebles, and N. C. Luhmann, Jr., "The use of polarization transforming reflectors for far-infrared and millimeter waves," Int. J. Infrared Millimeter Waves **7,** 1591–1603 (1986).